NACIONALNI INŠTITUT ZA BIOLOGIJO
MORSKA BIOLOŠKA POSTAJA

National Institute of Biology
Marine Biology Station Piran

Expert grounding for the implementation of the Marine Strategy Framework Directive (2008/56/ES) in Slovenia (2014).
Development of methodologies for evaluating effects on the ecosystem due to changes of hydrographical conditions in the sea environment – D7

December 2014

AUTHORS:

V. Malačič, U. Martinčič, B. Petelin (2014): Development of methodologies for evaluating effects on the ecosystem due to changes of hydrographical conditions in the sea environment – D7. In “Expert Grounding for the Implementation of the Marine Strategy Framework Directive (2008/56/ES) in Slovenia (2014)” (in Slovene). Final report in year 2014,152. Marine Biology Station, National Institute for Biology, Piran, 37 pp.

Table of contents

1. Expert grounding for the implementation of the Marine Strategy Framework Directive (2008/56/ES) in Slovenia (2014)

1.1. Development of methodologies for evaluating effects on the ecosystem due to changes of hydrographical conditions in the sea environment – D7

Introduction

From October to December we conducted long time series analysis by half-an-hour measurements of currents a couple of meters above sea bottom, right under the oceanographic buoy Vida. These analysis lead to ’reference values’ of the bottom stress, or the friction velocity, which will be concluded in 2015.
In accordance with this year's work plan we also placed some measuring equipment in the vicinity of the former shipyard in Izola. Prior to this we had to thoroughly test the devices, since the measuring instrument Vector was seriously damaged with a dragging net on August 19th 2014 in the Bay of Koper. Other equipment, exposed to hits and shocks, also had to be examined. We finished testing and placing the measuring instruments from October to December, including two Vector velocimeters (Nortek AS company) for measuring near-bottom currents with 16 Hz sampling), AWAC 1 MHz (Nortek AS) to measure currents over the whole water column (10 min averaging 1 s sampling), turbidity of sea water (Seapoint Sensors), the size distribution of resuspended sediment particles meter and the size distribution of in-situ measurements of settling velocities of suspended sediment meter (LISST-STX od Sequoia Instr.). After the setting the instruments were lowered to the bottom on December 12th 2014, around 9 m on the location DOK09 (13°40.054'E, 45°32.580'N), found 255 m west of the tip of the former Izola Shipyard pier. We started taking measurements at exactly 12.00 UTC time. These measurements will be representative for the open edge of the Viližan Bay conditions, the stated being an area of open interest for future sea interventions. The measurements will be concluded in January 2015 and analyzed in the same year. We also made an analysis of measurements at station KPTU2 (13°42.0'E,

45°33.70'N) conducted in July 2013 of distribution of sediment particles on their size and the distribution of the falling speed of particles on their size. We used the gathered data in the numerical model ECOMSED for sediment dynamics.

We conducted numerical simulation for sediment transport in the Bay of Koper with the ECOMSED model while the bora wind was blowing in the sinoptic time frame (three days).

An analysis of bottom currents measurements taken under Vida buoy

Introduction

From October to December we conducted the first long-term time series analysis of half-hour measurements of bottom currents under the oceanographic buoy Vida (13° 33,0' E; 45° 32,90' N; http://buoy.mbss.org) from November 2002 until the end of 2007 and from July 2008 until the end of October 2014. We did a seasonal statistics (three months averages) of currents speed distribution classifying them according to speed. We were also able to observe the seasonal variability of principal components of currents using the two-component PCA method. We ended the analysis with the variability of direction of principal axes along the vertical in order to see, how the direction of principal variances veers according to height above sea bottom – this is important in order to estimate the reasonability for the usage of logarithmic fit of vertical distribution of speed of near-bottom currents ; in case there is too much veering of direction according to height, it would probably be necessary to take into consideration the influence of Coriolis force in the bottom boundary layer, which leads to considerable complications in future analysis of calculating bottom stress by being forced to use Kelvin functions of zero'th order instead of logarithmic distribution (Soulsby, 1990; Cushman-Roisin and Malačič, 1997).

Method used in analysis of bottom currents' speed under buoy Vida

First we examined how many data were missing during the currents measurements in the interval from late October 2002 until end of October 2014. In 2002 and 2003 the currentmeter was set to measure in 20 cells of thickness 1 meter above the currentmeter, and in the next ten years in 21 cells of thickness 1 meter above the currentmeter. This fact influences the number of all expected data, which equals a total of 210940. The percentage of missing data from these is relatively high (13.0 %), while according to seasons, most of the data (16.5 % from 53548 expected data) is missing in the fourth (autumn) season (October – December) and the least in the second (springtime) season (10.2 % of 52416 data). The currents under buoy Vida were measured with an acoustic currentmeter 500 kHz ADP of the Nortek AS company from the end of October 2002 until the end of 2005, when we begun test-measurements of currents with a new acoustic currentmeter AWAC 600 kHz that also enables measurements of surface waves. In 2008, a new buoy Vida, made from stainless steel, was put in place. It worked uninterrupted until fall 2013 when we tug it out to the shipyard for refit after five years of operating. Between 2002 and 2007 we had to tug out the previous buoy on Vida's location each year for annual maintenance, which lead to the loss of one to two months worth of data. Both currentmeters measured currents in 10 min measurements every half hour. During those ten minutes the acoustic pulses were activated each second. After installing the AWAC currentmeter the 10 min measurements were followed by measurements of surface waves, by secondary set of pulses lasting 1024 s, which were also repeated every 30 min. By taking into consideration the height of the frame and the blank area right above the currentmeter, we can establish that in both cases the mid-height of the first cell was 2.3 m. The currents were measured with both currentmeters each meter of height. Since the goal of the analysis was to gain the values of bottom stress, we focused on the bottom four measurements of currents with the mid-height of the first cell 2.3 m and the mid-height of the last cell 5.3 m.

During the analysis we excluded all the currents' values that had speeds greater than 0.3 m/s, since it would be unrealistic to expect distinctive currents in the water body up to 5 m above bottom, at 22 m of depth. The statistics of the excluded values of currents that were too high shows that among all values from 2012 and 2014 (183438) the share of excluded values is 4.1%; regarding the seasons in the entire period the lowest share of excluded data is in the first, i.e. winter season (from the first to the third months), amounting to 2.1% of 46201 data, and the highest in the third, i. e. the summer season from seventh to ninth months in a year, when 6.0% of 45485 data were excluded, largely due to excluding data of high values in 2003 (22.8%) and 2007 (28.7%). The reason for these anomalies is yet unknown.

For the distribution frequency of speed of currents we decided to use classes of width 1 cm/s in the interval from 0 to 30 cm/s. We discovered that the distribution of frequency (number of occurrences) of speeds of currents follows very neatly the so called Weibull probability of density distribution (http://en.wikipedia.org/wiki/Weibull_distribition), which is described in the meteorological and oceanographic literature (Essenwanger, 1976; Emery and Thomson, 2001). The Weibull expression for the two-parameter probability density distribution is:

$$f(v)=\frac{\beta}{\alpha^{\beta}}v^{\beta-1}e^{-(v/\alpha)^{\beta}} \tag{0.1}$$

where f stands for number of measurements at current speed v, α and β are parameters of the Weibull distribution which we have to set with the non-linear fit of distribution of current speed on size classes.

Equating the derivation of (0.1) on v with zero ($df/dv = 0$) we get the position (speed v_0) of the velocity maximum:

$$v_0=\alpha\left(1-\frac{1}{\beta}\right)^{1/\beta}, \tag{0.2}$$

the maximum value f_0 of distribution at this velocity is:

$$f_0=\frac{\beta}{\alpha}\left(1-\frac{1}{\beta}\right)^{1-1/\beta}e^{\beta-1}. \tag{0.3}$$

Both expressions were used in writing out the statistics of speed distribution in Table 1, where we added a mean value of speed $\langle v\rangle$ and the standard deviation STD (v), which we calculated from the histogram of current speed values.

We performed calculation the above fit for each of the four cells above sea bottom, and from all the four cells at the same time. The Weibull probability density function has another elegant quality. The integral of (0.1) on speeds from zero to V

$$F(V)=\int_0^V f(v)\,dv=1-e^{-(V/\alpha)^{\beta}} \tag{0.4}$$

presents the cumulative distribution function and tells the probability at which speed values will be smaller than V. With known parameters α and β we can therefore easily calculate the probability that the values of speed v will be smaller than the chosen values V.

For the non-linear expression (0.1) we wrote the function in the Matlab software. The non-linear fit of data (Levenberg-Marquardt) with (0.1) requires (good) initial values for α and β that are to be determined by. These initial values were gathered using the “standard” call of function *‘wblfit’* in Matlab, which uses the maximum likelihood method. The entrance data at this call were the data from histogram of speeds on size classes of width 1 cm/s in the interval from 0–30 cm/s. The result of this call are (initial) values for α and β, as well as the fit, which leaves us discontented, since its maximum is at all times lower than the maximum of density distribution on speed classes, while the tail of the fit is too high. But we can still use gathered values for α and β as initial values for a completed non-linear fit using the least-square method, whilst again conducting a fit procedure on the histogram, but this time with an exterior function call instead of a call of *'wblfit'*. This procedure worked extremely well, so we decided to present results obtained by using this method.

Method of analysis of time and height variability of bottom currents

The variability of currents with time and height above sea bottom under the buoy Vida were separately treated for the time period 2002–2007, before changing the oceanographic buoy, and for the time period 2008–2014, after changing the buoy. The analysis showed that there were no significant differences between the two time periods. We therefore analyzed the variability of currents on the entire series of data from the end of October 2002 until the end of October 2014, using the same data we used for analyzing the distribution of speed of currents .

The time and vertical variability analysis is based on the calculation of the principal axes method with the two-component PCA (Principal Component Analysis) vector time series (Thomson and Emery, 2014; Preisendorfer, 1988), which is part of the empirical orthogonal functions (EOF) methods. Let us hereby write the groundwork which is based on searching for eigenvalues of the largest and the smallest variances of the eastern (u_e') and the northern component (u_n') of the time series of velocity$\mathbf{v}'$(t) = (u_e'(t), u_n'(t)) at one location at the same depth. We denote the fluctuations of velocity components as $u_e = u_e' - \langle u_e \rangle$, $u_n = u_n' - \langle u_n \rangle$. The co-ordinate system of currents is oriented so that the x-axis points towards East and the y-axis towards north, while the angle of inclination θ of the velocity fluctuation vector is increasing counter-clockwise from east. From these fluctuations the direction of principal axis θ_p is calcuated, alongside which the first maximum variance (first eigenvalue, or a principal value)of the vector of velocity fluctuations is present ($\theta_p = \theta_1$). Simultaneously, we also calculate the direction of the other axis, alongside which the smallest variance of velocity fluctuation is present ($\theta_p = \theta_2$). The latter, of course, is orthogonal to the axis with the largest variance. Let us presume that the velocity component along the first principal axis in the moment t_i is $u_1(t_i)$, and the velocity component along the second principal axis is $u_2(t_i)$. We can quickly demonstrate that $u_1(t_i)$ and $u_2(t_i)$ are linearly related with $u_e(t_i)$ and $u_n(t_i)$ with the transformation of axis rotation:

$$\begin{aligned} u_1(t_i) &= u_e(t_i)\cos\theta + u_n(t_i)\sin\theta \\ u_2(t_i) &= -u_e(t_i)\sin\theta + u_n(t_i)\cos\theta \end{aligned} \qquad (0.5)$$

We can write the variance of the vector along the eastern direction as

$s_{xx} = \sum_i u_e^2(t_i)/(N-1)$, where we summed squares of eastern velocity fluctuation component at moments t_i, where $i = 1\ldots N$ and N is the number of vectors. We can similarly write also the variance along the northern direction as s_{yy}, and the covariance as $s_{xy} = \sum_i u_e(t_i)u_n(t_i)/(N-1)$. We can thus write the speed fluctuation variance along the first principal axis s_1^2, and along the other principal axis s_2^2 from (0.5) as

$$\begin{aligned} s_1^2 &= \frac{1}{(N-1)}\sum_{i=1}^{N} u_1^2(t_i) = s_{xx}\cos^2\theta + 2s_{xy}\sin\theta\cos\theta + s_{yy}\sin^2\theta \\ s_2^2 &= \frac{1}{(N-1)}\sum_{i=1}^{N} u_2^2(t_i) = s_{xx}\sin^2\theta - 2s_{xy}\sin\theta\cos\theta + s_{yy}\cos^2\theta \end{aligned} . \tag{0.6}$$

Now we demand that s_1^2 is really the extreme variance, therefore the derivative of s_1^2 with respect to θ equals zero ($\mathrm{d}s_1^2/\mathrm{d}\theta = 0$) (Preisendorfer, 1988). By derivating (0.6) with respect to θ one obtains

$$(s_{yy} - s_{xx})\sin 2\theta + 2s_{xy}\cos 2\theta = 0 \tag{0.7}$$

from where the direction θ_1 of the first princial axis yields

$$\tan 2\theta_1 = \left(\frac{2s_{xy}}{s_{xx} - s_{yy}}\right) \Rightarrow \theta_1 = \frac{1}{2}\arctan\left(\frac{2s_{xy}}{s_{xx} - s_{yy}}\right), \tag{0.8}$$

and the direction of the second principal axis θ_2 with the lowest (if the first one was the highest) variance is orthogonal to θ_1: $\theta_2 = \theta_1 + 90°$.

Let us also calculate the principal values of the variances. We denote the largest ($s_{11} = s_1^2$) and the smallest ($s_{22} = s_2^2$) value of variances as eigenvalues (principal values). We are searching for the direction of the principal axis, or the direction along which the unit vector along the principal axis θ_p is stretched with the variance and is therefore dependent only on the eigenvalue λ along this axis:

$$\begin{bmatrix} s_{xx} & s_{xy} \\ s_{xy} & s_{yy} \end{bmatrix}\begin{bmatrix} \cos\theta_p \\ \sin\theta_p \end{bmatrix} = \lambda\begin{bmatrix} \cos\theta_p \\ \sin\theta_p \end{bmatrix} = \begin{bmatrix} \lambda & 0 \\ 0 & \lambda \end{bmatrix}\begin{bmatrix} \cos\theta_p \\ \sin\theta_p \end{bmatrix}. \tag{0.9}$$

This system of two equations only has a solution if its determinant equals zero

$$\begin{vmatrix} s_{xx}-\lambda & s_{xy} \\ s_{xy} & s_{yy}-\lambda \end{vmatrix} = 0\,, \qquad (0.10)$$

whence we get the quadratic equation for λ, and swiftly write its solution as:

$$\lambda = \frac{1}{2}\left[\left(s_{xx}+s_{yy}\right) \pm \sqrt{\left(\left(s_{xx}-s_{yy}\right)^2 + 4s_{xy}^2\right)}\right], \qquad (0.11)$$

where by placing the sign '+' in front of the root we get the highest variance, i. e. the first eigenvalue: $\lambda_1 = s_{11}$, while by placing the sign '-' we get the lowest variance $\lambda_2 = s_{22}$. We could obtain the expression for the eigenvalues (0.11) also by inserting θ_1 from (0.8) into the expression for variance (0.6), by which we first express $\cos 2\theta_p$ with the help of $\tan 2\theta_p$ from (0.8), that we use in $\cos^2\theta_p$, $\sin^2\theta_p$ and $\sin 2\theta_p$ in (0.6), whence it follows (0.11), with some calculation.

As we mentioned at the beginning, we used the PCA method to monitor the scatter of velocity vectors at the *chosen altitude* above sea bottom, which is a consequence of the(directional) variability of current vector at the chosen level. In this case the number of data pairs N for ($u_e(t_i)$, $u_n(t_i)$) is very large, over 10^4. But we also use this method for the *distribution of velocity vectors along the vertical* above sea bottom at *a chosen time*. In this case $N = 4$. The principal axes of this variability, especially their ratio between the lowest eigenvalue (the smallest variance) that means veering (or scattering) in the direction orthogonal to the direction with the largest velocity variance along the vertical, means veering the speed vector by height with regard to the first principal direction.

Then we calculate the mean value and the standard deviation of this ratio of eigenvalues of variances from the data of all measurements at different times, which is from over 10^4 eigenvalues of variance. The average value and the standard deviation of this ratio let us know if the current vector veering with height is important or we could disregard it in future analysis of vertical profiles of speed to calculate the bottom stress.

Results of the Weibull distribution of currents above the bottom under buoy Vida

Table 1 contains the results of the Weibull statistic of currents speed. In all the cases the fit was in good agreement with the data, R^2 never dropped below 0,993.

Table 1. Weibull statistic of velocity distribution in cells 1 (2.3 m above the bottom) to 4 (5.3 m above the bottom). The season means a consecutive number of the trimester in the year, α and β are parameters of distribution, v_0 is the most frequent speed, $f(v_0)$ the value of distribution maximum, N the number of used values, $\langle v \rangle$ is the average value of speed and STD (v) is the standard deviation of speed. The time period of measurement is November 2002–October 2014.

Season	Cells	α (cm/s)	β	v_o (cm/s)	$f(v_0)$	R^2	N	$\langle v \rangle$ (cm/s)	STD (v) (cm/s)
1	1	7,25	1,845	4,75	0,11	0,997	45897	6,71	4,16
1	2	7,59	1,818	4,89	0,11	0,997	45926	7,03	4,33
1	3	7,89	1,794	5,01	0,10	0,996	45964	7,30	4,52
1	4	8,08	1,788	5,11	0,10	0,995	45964	7,49	4,64
1	1-4	7,68	1,808	4,92	0,11	0,996	183751	7,13	4,43
2	1	8,07	1,880	5,39	0,10	0,997	46640	7,41	4,42
2	2	8,72	1,825	5,64	0,09	0,996	46657	8,01	4,82
2	3	9,04	1,809	5,79	0,09	0,996	46638	8,29	5,01
2	4	9,18	1,811	5,89	0,09	0,996	46643	8,44	5,09
2	1-4	8,73	1,827	5,66	0,09	0,997	186578	8,04	4,86
3	1	9,10	1,882	6,08	0,09	0,998	44558	8,31	4,87
3	2	9,72	1,827	6,30	0,08	0,997	44917	8,86	5,22
3	3	10,06	1,775	6,31	0,08	0,996	44856	9,17	5,48
3	4	10,13	1,785	6,40	0,08	0,993	44848	9,29	5,53
3	1-4	9,73	1,814	6,25	0,08	0,996	179179	8,91	5,30
4	1	7,91	1,845	5,18	0,10	0,995	44044	7,39	4,59
4	2	8,21	1,826	5,32	0,10	0,994	44151	7,68	4,78
4	3	8,35	1,825	5,40	0,10	0,993	44171	7,80	4,82
4	4	8,42	1,819	5,43	0,10	0,994	44190	7,85	4,86
4	1-4	8,21	1,829	5,33	0,10	0,994	176556	7,68	4,77

An additional analysis of parameters α and β while performing non-linear fits shows that the deviation around the 'true' value of the parameter α, or the 95% confidence interval for its value around the central (fit) value is, in all cases, ±0.18 at most. Therefore, writing the value for α to two decimals places is more than sufficient; the first decimal place is reliable. For the parameter β the confidence interval is at most ±0.04 wide, so writing out the value at three decimals is more than sufficient, the second decimal place is hardly reliable. The typical value for β is 1.8, while for α it is somewhere between 7.3 cm/s to 10.1 cm/s. Let us calculate the probability that the speeds are lower than the chosen speed according to (0.4). With the pair of values α = 7,3 cm/s and β = 1,8 the probability that the speed will be lower than 10 cm/s equals 82.8%, and that it would be lower than 20 cm/s it equals

99.8%. With the pair of values α = 10,1 cm/s and β = 1,8 the probability that the speed would be lower than 10 cm/s equals only 62.6% and that the speed would be lower than 20 cm/s equals 96.7%. We can conclude that at most 3.3% of velocities are larger than 20 cm/s, and only in the third, summer season (July-September) with the fourth cell at the height of 5.3 m. In all other cases of trimesters and heights this percentage is lower than 3.3%. The lowest is the share of all speeds (0.2 %), that are higher than 20 cm/s in the case of the first cell above the bottom at the height of 2.3 m in the winter season (January-March).

The most frequent velocity currents v_0, as well as the mean velocity of currents $\langle v \rangle$, and its standard deviation STD(v) increase with the height above the bottom, marked with the consecutive number of cells above the bottom in Table 1. It was surprising that the lowest values for $v_{0,}$ $\langle v \rangle$ and STD(v) were present in the first, winter trimester (January–March) and the highest values in the third, summer trimester (July–September). The most frequent velocity v_0 2,3 m above the bottom (first cell) is found in the interval between 4.8 cm/s and 6.1 cm/s, and the $\langle v \rangle$ between 6.7 cm/s and 8.3 cm/s. At 5.3 m above the bottom (fourth cell) v_0 is between 5.1cm/s and 6.4 cm/s, while $\langle v \rangle$ is between 7.5 cm/s and 9.3 cm/s. STD(v) is limited to values between 4.2 cm/s and 5.5 cm/s.

Figure1 shows a typical Weibull distribution of velocity.

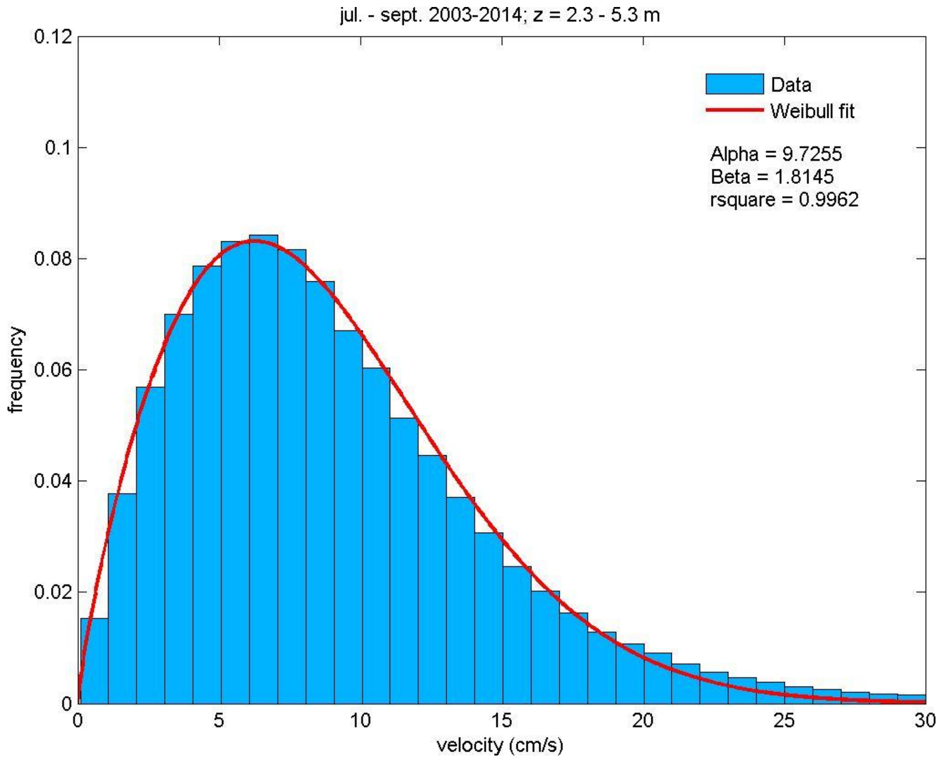

Figure 1. Velocity distribution of currents between 2.3 m to 5.3 m above the bottom under the buoy Vida for the third trimester (July – September).

Results of the PCA analysis of the variability of bottom currents

The time variability of bottom currents at different levels is gathered in Table 2. We can see that the square roots of the principal variances ($s_1 = (s_{11})^{0.5}$, $s_2 = (s_{22})^{0.5}$), which represent a measure for the "principal standard deviations", are steadily increasing with height (consecutive number of cells) in all seasons. The ratio of the 'principal standard deviations' s_2/s_1, rounded up to one decimal place, almost always equals 0.6, except in four cases, when the rounded value equals 0.7.

Table 2. Directions of the principal axis θ_1 of the highest variance, square roots of the principal variances s_1 and s_2, the mean values of bottom currents and their direction φ with respect to the east.

season	cell	N	θ_1 (°)	s_1 (cm/s)	s_2 (cm/s)	s_2/s_1	$\langle u_e \rangle$ (cm/s)	$\langle u_n \rangle$ (cm/s)	φ (°)
1	1	45912	30.3	6.6	3.9	0.58	1.8	-0.3	-9.4
	2	45935	30.1	7.0	4.0	0.57	1.8	-0.2	-6.9
	3	45972	30.1	7.3	4.1	0.56	1.9	-0.2	-6.9
	4	45972	30.3	7.5	4.1	0.55	1.9	-0.2	-6.8
2	1	46648	32.1	7.2	4.7	0.66	0.3	-0.4	-53.2
	2	46663	28.4	7.9	5.0	0.64	0.2	-0.3	-53.3
	3	46647	27.3	8.1	5.2	0.65	0.4	-0.2	-29.3
	4	46655	27.2	8.2	5.5	0.67	0.6	-0.3	-23.2
3	1	44565	31.8	8.0	5.1	0.64	1.2	-0.6	-26.0
	2	44924	27.5	8.6	5.5	0.63	1.1	-0.5	-24.3
	3	44865	25.1	8.9	5.8	0.65	1.3	-0.4	-16.6
	4	44857	24.9	8.8	6.1	0.69	1.4	-0.2	-10.1
4	1	44049	30.2	7.3	4.3	0.58	1.9	-0.5	-14.2
	2	44158	29.4	7.7	4.4	0.57	1.9	-0.5	-13.3
	3	44180	28.7	7.8	4.4	0.57	1.9	-0.4	-10.8
	4	44203	28.5	7.9	4.4	0.56	1.9	-0.4	-11.1
all	1	181174	30.9	7.3	4.5	0.62	1.3	-0.4	-19.1
	2	181680	28.5	7.8	4.8	0.61	1.3	-0.4	-16.3
	3	181664	27.4	8.1	4.9	0.61	1.4	-0.3	-12.3
	4	181687	27.5	8.1	5.1	0.63	1.4	-0.3	-10.8
	all	726205	28.5	7.8	4.8	0.62	1.3	-0.3	-14.5

The direction of the principal axis with the largest variance of time variability of currents is around 28.9° ± 2.1°. This range embraces values of the principal axis direction in each of all cells and each of all seasons. We can conclude that the variance is directed along the axis of the Gulf of Trieste. It is interesting to note that the velocity of time average of currents (not shown here, we calculate it from $\langle u_e \rangle$ and $\langle u_n \rangle$), does not rise with the height above sea bottom, but its values are between 0.4 and 2.0 cm/s, or rather, its mean and standard deviation are: 1.4 cm/s ± 0.07 cm/s.

The direction of the mean current is much more variable than the direction of the principal axis: the direction of the mean current in all seasons can be found in the interval between -53.3° and -6.3°, or -14.6° ± 3.8° (Table 2, last column, four values above the value in the last row were used), so all the values belong to the fourth quadrant, therefore in the direction toward southwest, i e. from buoy Vida towards Fiesa and Strunjan.

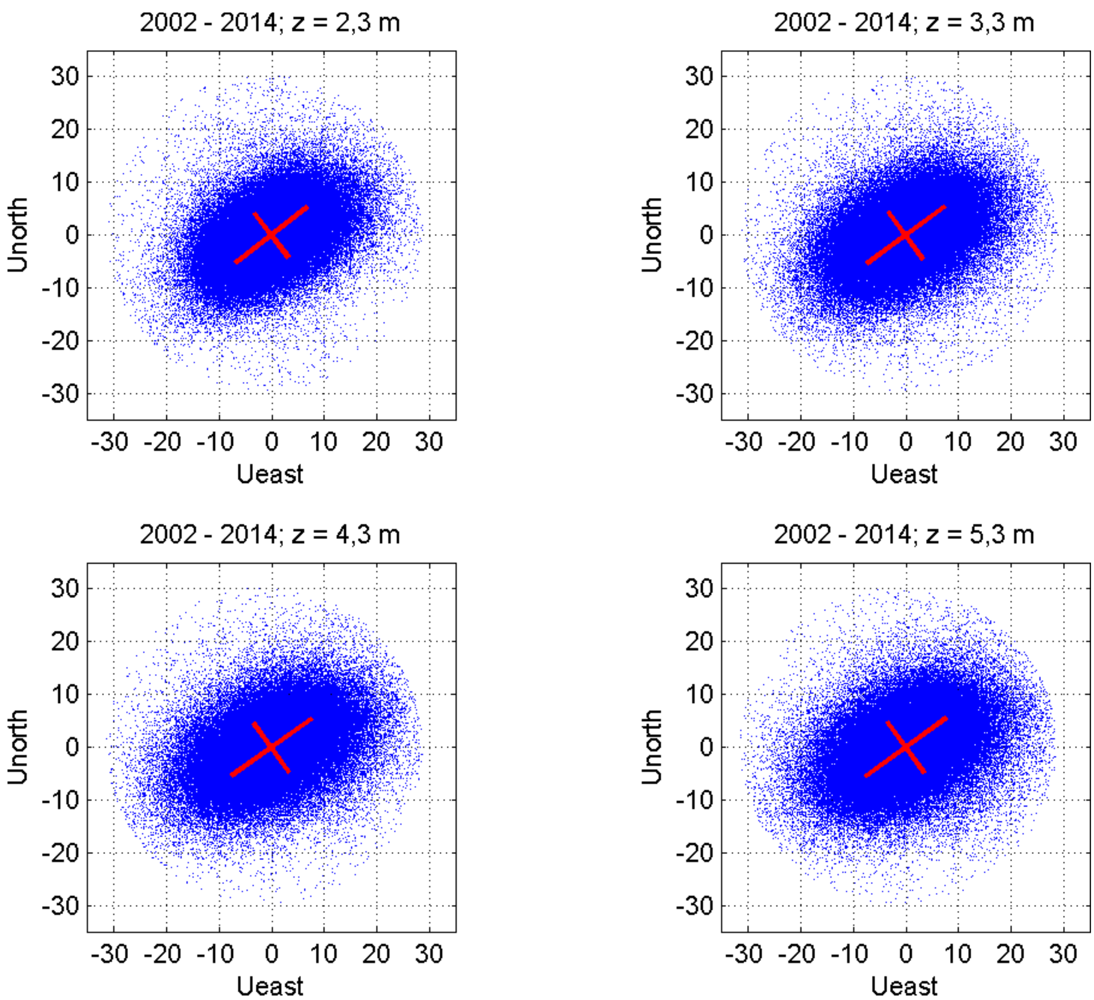

Figure 2. Distribution of fluctuations of velocity vectors in clouds at different heights above the sea bottom from measurements taken between 2002 and 2014, where all the seasons were united. The red cross in the middle of plots illustrates the principal standard deviations along the principal axes of velocity fluctuation clouds.

Figure 2 shows velocity fluctuation clouds and the principal standard deviations of clouds along the principal axes. We observe a considerable steadiness of the direction of the principal axis from one height to the other, and we can find values in Table 2 that correspond to different clouds (the lines next to the "all" seasons column).

The vertical variability of the principal axes is presented in Table 3. The essential finding here is that in all seasons the ratio of the second and the first principal standard deviations is 0.2 ± 0.2, meaning that the mean value of the ratio between the lowest and the highest standard deviation equals 1/5 due to changes of direction. This means that the currents in all four cells above the bottom are practically in one vertical plane, even in the layer above the bottom, where we can presume that the change of the direction of currents along the vertical is not important and that we can disregard the veering of the current vector in future calculations of friction velocity. We will therefore calculate the bottom stress from the vertical distribution of current velocities, as is usual to do with currents in places where the direction virtually never changes along the vertical (e.g. in rivers).

Table 3. Mean values of principal axes, which show the variability along the vertical distance from the sea bottom. At every instant of measurements the PCA method was used on four current vectors in four cells of different heights above the bottom. Mean standard deviations and their ratios, as well as the time average of these ratios and their standard deviations in time are calculated from all instantaneous PCA's.

Sezona	N	$\langle s_1 \rangle$	$\langle s_2 \rangle$	$\langle s_2/s_1 \rangle$	STD(s_2/s_1)
1	45535	9.23	1.40	0.21	0.19
2	45977	16.45	2.22	0.20	0.19
3	43560	20.13	2.48	0.19	0.18
4	43167	13.63	1.69	0.21	0.19

We demonstrate the principal direction variability along the vertical with Figure 3, which is otherwise another reflection of the results in Table 2. As we can see, the average currents are directed towards southwest (towards Strunjan) and the direction of the principal axis hardly changes with height, while the ratio of principal axes is 0.6.

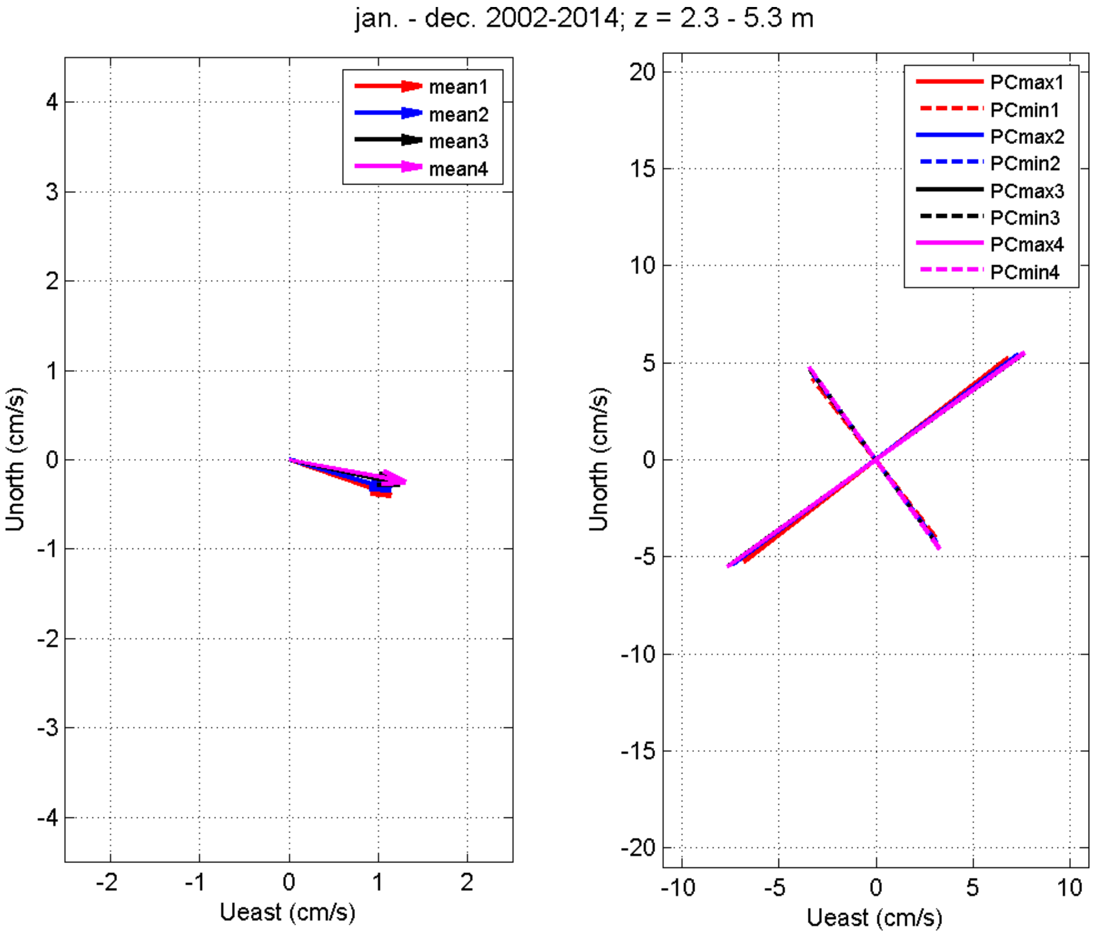

Figure 3. Left: Distribution of time average of current vectors with height in four cells above the bottom. Cell 1 is at height 2.3 m above the bottom and cell 4 is 5.3 m above the bottom. Right: Distribution of principal standard deviation of currents with height.

Measurements of settling speed of sediment particles above the sea floor

Introduction

For the numerical model of sediment transport we used the results of measurements of settling speed of sediment particles, which were found in a water column above the sea floor. For this purpose we examined the most reliable measurements we have so far. We analyzed measurements in the period from July 23rd to July 31st 2013, when the LISST-STX measuring instrument (LISST = Laser In-Situ Sediment Size Transmissometer) was operating at station KPTU2 (13° 42.0' E, 45° 33.7' N) in the middle of the Bay of Koper, about 0.3 m above the bottom in the depth of 19 m below the shipping lane. Besides monitoring the distribution of volume concentration on size of sediment particles re-suspended in the water column, the LISST-STX instrument also enables the monitoring of distribution of settling speed of sediment particles on size of sediment (floating) particles.

Measuring method with LISST-STX

LISST's functioning is based on the scattering image of the red-light laser beam (670 nm), which scatters on (sediment) particles in a sea-water in a chamber at the bottom of the settling tower. The distribution of scattered laser light on detectors at the other side of the chamber, which are placed in 32 circular rings, yields the information about the volume distribution of sediment particles in 32 size classes of particles, with their median values in the interval from 1,36 μm to 230 μm. The size of particles is the median dimension of particles, which corresponds to the radius of spherical particles of the same volume.. Suspended particles can be of different shapes, for example needle- or stick-shaped, or plate-like. From LISST's measurements it is not possible to discern their shape. If the same water mass is held up in the settling tower, it is possible to also gain the speed distribution on particle sizes from several consecutive snap-shots of the scattering image in periods of unequal time intervals, which are clearly determined. But the distribution of the falling speed can only be determined for larger size classes, which means a smaller number of size classes (eight), with medial diameters from 1.74 μm to 180 μm. To determine the smallest grains in the size range of 2-3 μm it is necessary that the same water mass is held up in the settling tower for at least 22 hours (83 scan-images) and almost 9 hours (66 scan-images) to determine the settling speed of particles sized 3-4 μm.

In the afore mentioned period from July 23rd to July 32nd 2014 we managed to extract from the LISST-STX measurement five useful series of laser scans, where all 83 scans were completed and 66 scans in the last, uncompleted set of measurements, cumulating to 481 settling distributions. With this number of measurements we calculated the medial size of the grains' diameter in each of the 32 classes. The statistics of particle settling speed distribution on median grain size is calculated from thethe five complete series of settling images.

Results of the LISST-STX measurements

Figure 4 shows the distribution of the re-suspended sediment particles on grain size (left plot). We observe two peaks, one around 8–10 μm (clay-silt), and the other, a lot smaller peak with a much higher variability of peak height (a high standard deviation), at around 50–60 μm. The right plot of Figure 4 shows the settling speed distribution. The settling speed is growing with particle size in log-log plot, but it does not grow linearly; the increase in speed with particle size is lower in the area around 20–30 μm.

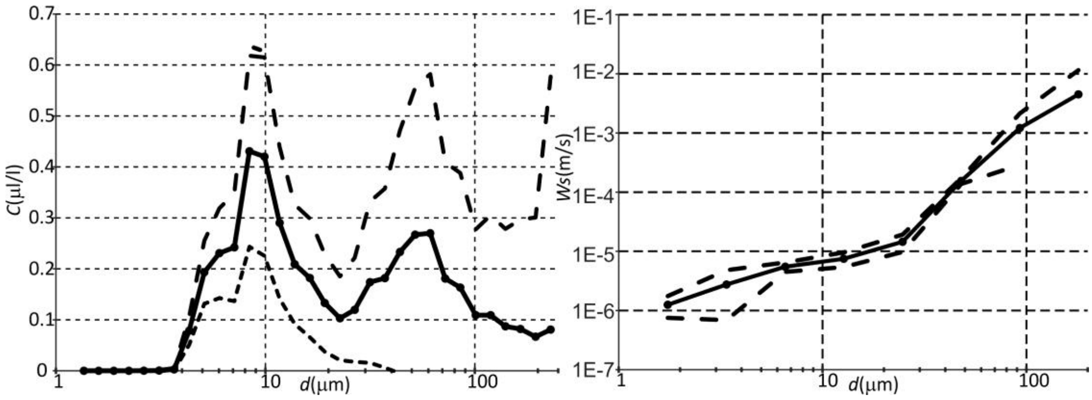

Picture 4. Left: Distribution of volume concentration of particles about 0.3 m above the sea-bottom. Right: distribution of settling speed of particles. Full line: average values. Dashed line limits scattering around average value for one standard deviation above and under the average value, where the lower limits, made negative with this calculation, are not shown. Average values and standard deviations of particle size distribution are made from 581 values, while the speed distribution is calculated only from five values (the five whole sets of scattering images).

In the stated ranges of grain diameters, where we get two peaks in particle size distribution, the median value of the size class for settling speed distribution, matching the first peak of particle size distribution, equals 12.7 μm, while the correspondent settling speed is 7.5 10^{-6} m/s. The second median value of grain size for the settling speed distribution, which is matching the second peak of particle size distribution, equals 47.9 μm, while the corresponding settling speed at this size is for two orders of magnitude larger, equal to 1.55 10^{-4} m/s.

Simulation of sediment dynamics in the Bay of Koper during the Bora wind (ECOMSED)

Introduction

We set two circulation (forecast) models for the Bay of Koper and the Bay of Piran, with a horizontal resolution of 37 m, that are based on the Princeton Ocean Model (Blumberg & Mellor 2013). Both models are nested in the model of the Gulf of Trieste with a horizontal resolution of 150 m (Figure 5), while the latter is also nested in the model of the Northern Adriatic with a horizontal resolution of 600 m. Resulting sea surface elevation, temperature, salinity and currents are issued from these two models of wide-open bays in the 25 vertical sigma levels. Furthermore, we can also gather data on bottom stress due to bottom currents.

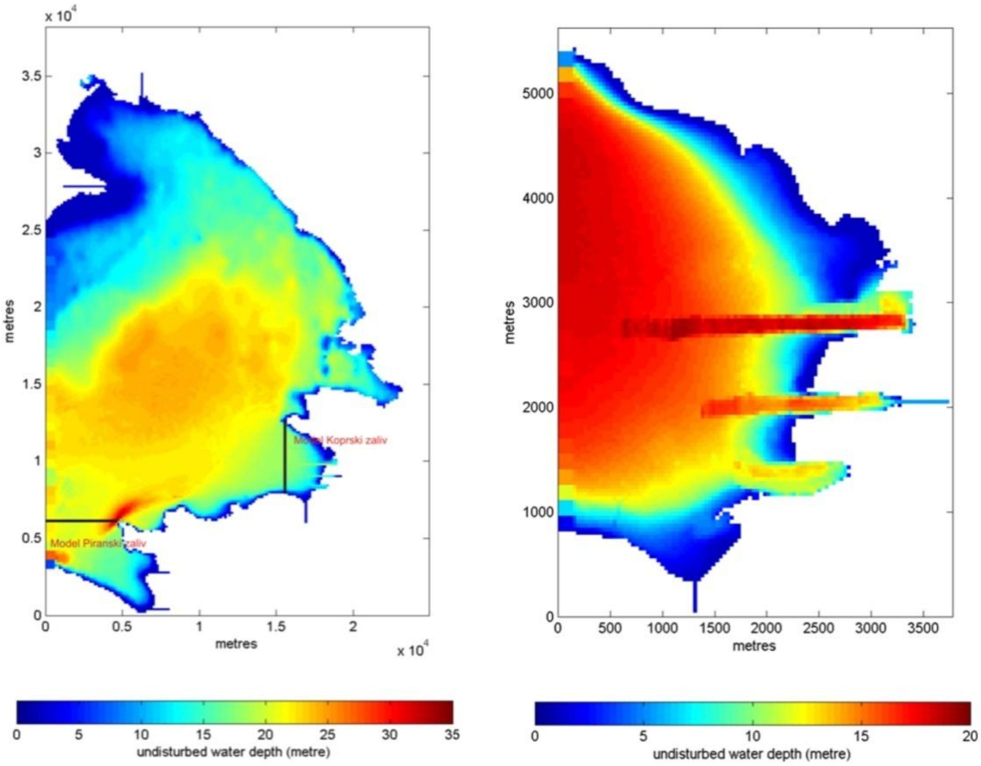

Figure 5. Left: Domain of the circulation model for the Gulf of Trieste, where the two models for the Bay of Koper and the Bay of Piran are placed. The open edge of both nested models is marked with a black line. Right: Domain of the circulating model for the Bay of Koper. The color bar at the bottom of plots represents the bottom depth.

Alongside the circulating models we also placed a sediment transport module of the model ECOMSED (HydroQual n.d.), which simulates the dynamics of the surface

sediment at the sea bottom and in the water column, into which we inserted the data of currents, calculated with the aforementioned circulation model for the Bay of Koper (Figure 5, right plot).
ECOMSED also calculates the bottom stress data due to currents and surface waves for both, cohesive and non-cohesive sediments. It also records changes in the depht of sediment surface, sediment thickness and the concentration of sediment particles in the water column at various depths.

Methods of numerical simulations

Both models (the circulation model and ECOMSED) ran for typical synoptic situations during the Bora wind, as well as during calm weather with tides. We also conducted a comparison of the results of the circulation models for the Bays of Koper and Piran with currentmeter measurements during clement weather. We discovered that model results during clement weather largely deviate from measurements due to false boundary conditions that the model collects from the model for the Gulf of Trieste – and the latter is retrieving them from the model for the Northern Adriatic. We will demonstrate the results of the ECOMSED model for the Bay of Koper in the case of the Bora wind blowing from 19th March 2014 to 21st March 2014. The Bora wind started blowing on the 19th March at 18:00 with an average speed of 9.8 m/s from the direction (azimuth) 77.6° until the end of 21st March.

At our first simulation with the model ECOMSED for the Bay of Koper we had to determine the proper model parametrization of sediment properties, which is more demanding for cohesive than for non-cohesive sediments. During this phase we followed a prescribed method (Cardenas et al. 2005); the choice of model parameters influences the calculations of the bottom friction coeficient as well as rising and settling speeds of cohesive sediments. The settling speed of cohesive elements w_s (m/day) is calculated with the expression:

$$w_s = \alpha (CG)^{\beta} \tag{0.12}$$

where the two parameters are α = 2.42 and β = 0.22, C is the concentration of the cohesive suspended sediment (in mg/l = 10^{-6} g/cm^3 = 10^{-3} kg/m^3)and G is the internal shear stress (in dyne/cm^2 = 0,1 Pa) that influences the agglomeration and settling of particles and is calculated as:

$$G = \rho K_M \left[\left(\frac{\partial u}{\partial z} \right)^2 + \left(\frac{\partial v}{\partial z} \right)^2 \right]^{1/2}, \tag{0.13}$$

where ρ is the density of the sea water with the sediment, K_M is eddy viscosity, and (u,v) are horizontal components of speed that change with height z at the given location. Flux density of sedimentation (deposition) in the bottom layer is written as:

$$D = -w_s C P, \tag{0.14}$$

where D stands for the mass flux density of sedimentation (g/(cm^{2}s)), the speed of settling w_s is now in cm/s, while the concentration of sediment C is in mg/l, with P being the probability of settling. Complicated expressions have been developed for the latter, also used also in the ECOMSED model; here we state the least complicated one (Krone, 1962):

$$P = \begin{cases} 1 - \dfrac{\tau_b}{\tau_d}; & \tau_b \le \tau_d \\ 0; & \tau_b > \tau_d \end{cases}, \tag{0.15}$$

where τ_d is the critical stress for settling, found in the range between 0.6 and 1.1 dyne/cm^2 (HydroQual, 2014).

The mass of the elevated (eroded) sediment per unit of horizontal surface ε (unit mg/cm^2) depends on the difference between the bottom stress τ_b (unit dyne/cm^2 = 0.1 Pa) and the critical stress τ_c required for the erosion of the cohesive sediment. The mass of elevated sediment appears in the water above the bottom in roughly one hour (HydroQual, 2014), which we have to take into consideration while calculating the density of flux density of mass of sediment erosion E_{tot} (mg/(cm^{2}s)), which means elevating of the mass of the cohesive sediment per unit of horizontal surface per unit time(Krone 1962). The flux density of mass and the lifted mass per unit of surface are calculated with these equations:

$$\varepsilon = \frac{a_0}{T_d^m}\left(\frac{\tau_b - \tau_c}{\tau_c}\right)^n \qquad E_{tot} = \frac{\varepsilon}{3600\,\mathrm{s}} \tag{0.16}$$

where we adopted values for coeficients a_0 = 1.6 mg/cm^2, n = 2.5 and m = 0.8 (Cardenas et al. 2005), τ_c = 1 dyne/cm^2 (= 0.1 Pa). T_d is time in days since the last settling (deposition) of sediment to the bottom, that elapsed until the discussed resuspension. Trials have shown that the τ_c has values in the interval from 0.06 to 0.11 Pa. We used the mean value 0.085 Pa.

At the second experiment we inserted into the ECOMSED the typical vertical speeds (w) of settling of sediments for the two typical sizes (d) of grains: d_1 = 12.7 μm, w_1 = 7.50·10^{-6} m/s and d_2 = 47.9 μm, w_2 = 1.55·10^{-4} m/s. These values for grain sizes and settling speeds were retrieved from the previously described measurements we made with LISST-STX instrument.

We tested the influence of waves on the bottom shear stresses and sediment elevation. In the first case, waves were calculated with the help of a procedure built in the ECOMSED (Donelan, 1977). In the second case we interpolated into the model for the Bay of Koper the waves from the results of the SWAN (Delft TU n.d.) model, which was set on the domain of the circulation model for the Northern Adriatic with a horizontal resolution of ~600 m.

Results of the numerical simulations

Model results have shown that the SWAN model for the Northern Adriatic is unsuitable to monitor wave conditions in the Bay of Koper, because coarse model grid in the SWAN model (600 m) caused that coastal sea-cells can contain a significant patch of land, where sea actually resides, or they contain a too high percentage of sea with an average depth of sea cells where land is actually present. These are important areas around the peaks of the peers in Luka Koper (the Port of Koper) in the inside part of the Bay of Koper area, where the variability of depth is very distinctive due to shipping channels, and in the coastal northern and southern parts of the Bay of Koper. In calculations that included the procedure, built in the ECOMSED (Donelan 1977), that is based on the calculation of waves from wind data, that have to be separately inserted into ECOMSED's programme, we were, unfortunately so, unable to gain any useful results, or results that would logically increase the bottom stress. So we have to validate these results with additional experimental or numerical results.

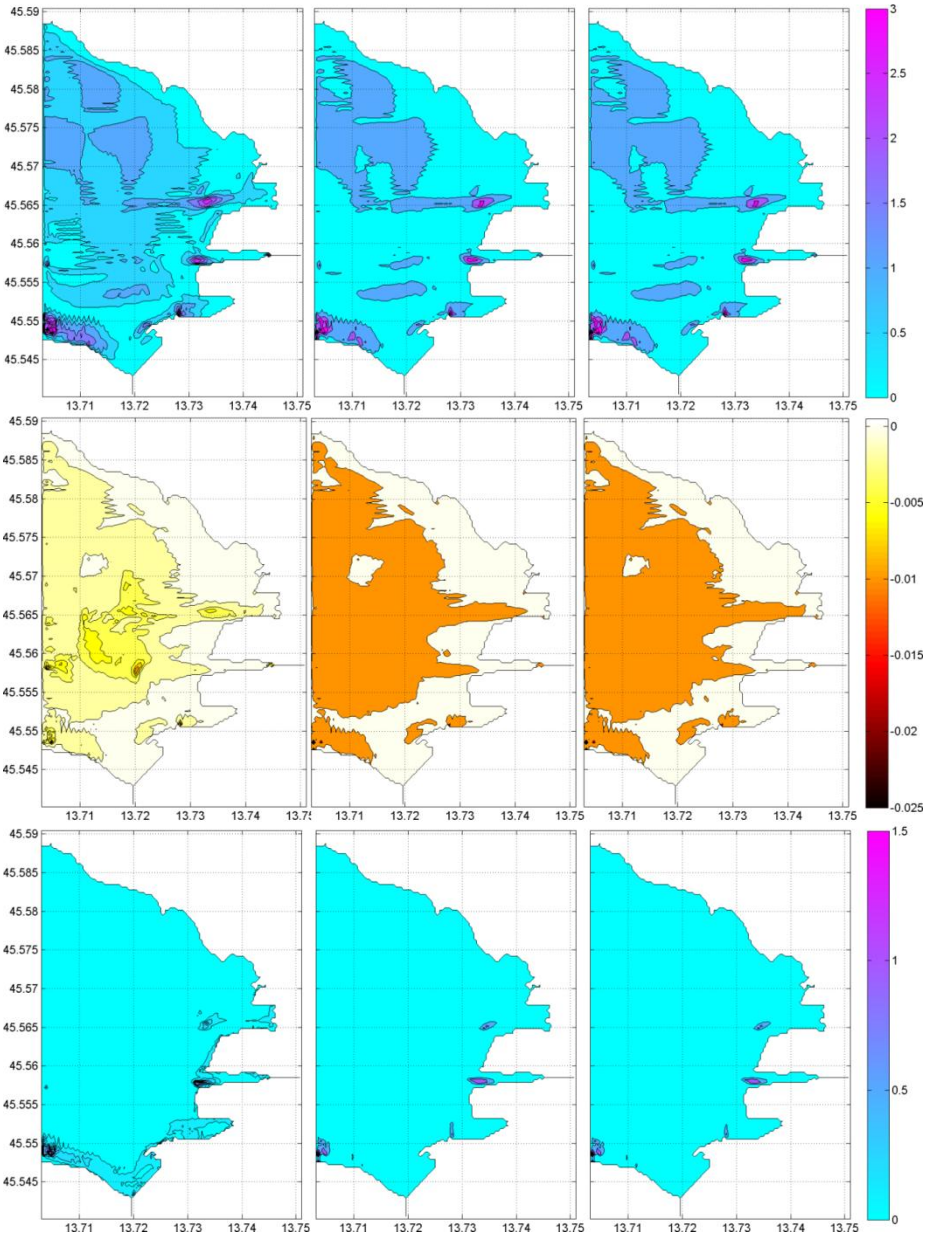

Figure 6. Results of the ECOMSED model after the ceasing of the Bora wind from 19th March 2014 to 21st March 2014: Top row: shear stress at the bottom (dyne/cm^2). Middle row: changes of heights of the cohesive sediment (cm). Bottom row: concentration of the cohesive sediment in the water at the bottom (mg/l). Left column: settling speed of sediment in the water close to the bottom, calculated in the ECOMSED; middle column: settling speed $1.55 \cdot 10^{-4}$ m/s ; right column: settling speed $7.50 \cdot 10^{-6}$ m/s.

Figure 6 shows the distribution of the bottom stress (top row) after three days of the Bora wind blowing from March 17th – 19th 2014. Small areas of distinctively increased stress are clearly visible at the beginnings of the canals between the peers of Luka Koper along their southern side. A slightly bigger area of increased bottom stress is also visible at the southern coast of the Bay of Koper, close to the open edge of the model area, a location where we cannot yet trust the results due to coupling with the larger and coarser model and they have to be checked with additional simulations. The increased bottom stress at the locations on the openings of the canals between the piers is present in all three simulations of settling speed of sediments in the bottom layer above the sediment, regardless of the used method, so it appears as a reliable result. In the middle row of plots we can observe the lowering height of the bottom sediment (sweeping away the sediment from the bottom) in the Bay of Koper due to the Bora wind. When the model calculates settling speeds by itself in the simulations of sediment transport without the prescribed settling speeds (left column of plots), we can observe the highest lowering of sediment height (erosion) at the end of the deepening of the shipping channel (compare Figure 5 (right) with Figure 6 (left, second row), which is a logical result. The bottom row of plots shows, regardless of the chosen method of settling, that sediment concentrations at the bottom are raised in places with elevated bottom stress, which is in the southern parts of the canal openings between the pears and in the proximity of the open boundary along the southern coast, where higher concentrations have yet to be examined further, as aforementioned in the description of the bottom stress distribution.

Conclusion and directions in 2015

In 2014 we conducted the analysis of measurements of bottom currents under the buoy Vida, which will be followed in 2015 by the first statistical distribution of ‘reference value’ of the friction velocity and bottom stress under the buoy Vida from archived measurements of currents made from 2002 to 2013. We discovered that the eigenvalues and directions of the principal axes of the time variance of currents do not change significantly with height, while the eigenvalues of the vertical variability have, in the average time, a ratio of 1/5 between the lowest and the highest standard deviation along the principal axes. This means we can disregard the variability of current direction by height when we will continue with the analysis of bottom currents, leading to calculations of the bottom stress. In 2015 we will also conduct a corellation of calculations with waves (surface waves) and perhaps with the tides (tidal range around 1 m), if we estimate that the latter has considerable influence on the modulation of the bottom stress.

In 2014 we placed two models for circulation in the bays of Koper and Piran, and set into action the model of sediment transport ECOMSED for the Bay of Koper. We found isolated areas of elevated bottom stress in front of the canals of Luka Koper and elevated concentrations of sediment in the water above the bottom. Regarding the numerical simulations of the sediment transport we will conduct a calculation of waves in 2015, using the SWAN model with a high resolution in the model domain for the Bay of Koper, so we might be able to compare the results of the ECOMSED model with the results of the PCFLOW3D model, which is run by the Faculty of civil and geodetic engineering of the University of Ljubljana, Fluid mechanics laboratory.

In 2015, we will conclude the analysis of near-bottom high-frequency (16 Hz) measurements of currents and turbidity, that were conducted at the station KPTUR (13°40.00' E, 45°35.00' N, bottom depth over 20 m) on the shipping lane from 12th August 2014 at 12:00:00 until 19th August 2014 that are under the influence of the marine traffic. We will also conclude the analysis of measurements currently taking place at the entrance of the Viližan bay at the station DOK09 (13°40.054'E, 45°32.580'N). In 2015 we also anticipate the installation of measuring devices under the buoy Vida, which will enable us to evaluate calculations of the bottom stress from the vertical profile of time average of currents (in 10 min intervals every 30 min) close to the sea bottom with the direct measurements of fluctuations of the bottom currents, which are used to calculate the bottom stress.

2.

SOURCES

Blumberg, A.F. & G.L. Mellor (2013): A Description of a Three-Dimensional Coastal Ocean Circulation Model. In N. S. Heaps, ed. *Three-Dimensional Coastal Ocean Models*. American Geophysical Union, pp. 1–16. Available at: http://dx.doi.org/10.1029/CO004p0001.

Cardenas, M.P. *et al.* (2005): Sediment Transport Model Validation in Lake Michigan. *Journal of Great Lakes Research*, 31, pp.373–385.

Cushman-Roisin, B. & V. Malačič (1997): Bottom Ekman Pumping with Stress-Dependent Eddy Viscosity. Journal of Physical Oceanography 27, 1967-1975 str.

Delft TU, SWAN. Available at: http://www.citg.tudelft.nl/over-faculteit/afdelingen/hydraulic-engineering/sections/environmental-fluidmechanics/research/swan/ [Accessed December 3, 2014].

Donelan, M.A. (1977): *A simple numerical model for wave and wind stress application*, Burlington, Ontario, Canada.

Emery, W.J. & R.E. Thomson (2001): Data Analysis Methods in Physical Oceanography. Amsterdam: Elsevier.

Essenwanger, O. (1976): Applied Statistics in Atmospheric Science. Part A. Frequencies and Curve Fitting. Amsterdam: Elsevier.

HydroQual, I., ECOMSED. Available at:

http://www.hydroqual.com/ehst_ecomsed.html [Accessed December 3, 2014].

Krone, R.B. (1962): *Flume Studies of the Transport of Sediment in Estuarial Processes*, Berkeley.

Preisendorfer, R.W. (1988): Principal Component Analysis in Meteorology and Oceanography. Amsterdam: Elsevier.

Soulsby, R. L. (1990): Tidal-Current Boundary Layers. In *The Sea*, Vol. 9, Part A, Ocean Engineering Science, 523-566 (Eds B. LeMehaute and D. M. Hanes). New York: Wiley Interscience.

Thomson, R.E. & W.J. Emery (2014): Data Analysis Methods in Physical Oceanography. Amsterdam: Elsevier.